

# A novel approach to motion tracking with wearable sensors based on Probabilistic Graphical Models

Emanuele Ruffaldi<sup>1</sup> and Lorenzo Peppoloni<sup>1</sup> and Alessandro Filipposchi<sup>1</sup> and Carlo Alberto Avizzano<sup>1</sup>

**Abstract**—Wearable motion tracking systems represent a breakthrough in ecological motion tracking. Their effectiveness has been proved in many fields, from performance assessment to human-robot interaction. Most of the approaches are based on the exploitation of optimal probabilistic filtering of inertial motion units (IMUs) signals, ranging from linear Kalman Filters (KF) to Particle filters (PF). Since most of the models are highly nonlinear, filters such as Extended Kalman Filter (EKF) and Unscented Kalman Filter (UKF) are typically used. These approaches cause all the variables of the models to be correlated each other. Probabilistic Graphical Models (PGM) are a framework for probabilistic reasoning that allows to explicitly declare the actual dependencies among variables. In this paper we propose a novel algorithm for motion tracking with IMUs based on PGM. The model is compared to the state of the art UKF algorithm in tracking the human upper limb. The results show that the proposed approach perform a slightly better compared to the UKF.

## I. INTRODUCTION

Human motion tracking has been vastly studied in the last decades for its applications that span from performance assessment to human robot interaction. Traditionally motion tracking is based on optical capture systems. Those systems show a great degree of accuracy but suffer from occlusions and are sensitive to changes in lighting conditions, moreover their usually small workspace does not make them suitable for outdoor tracking. These issues are overtaken by wearable motion tracking systems. Among all the approaches those based on IMUs have gained popularity in this research field being self contained, and unobtrusive. The main drawback of this approach is the impossibility of directly integrating IMUs data because of drift. To overcome this problem several filtering and sensor fusion techniques have been studied, among all the most used techniques are based on Bayesian filters. According to the complexity of the problem considered two different families of approaches can be identified, the first comprises linear filters such as Kalman Filter (KF). Those are used for example in the case of simpler models which consider every limb independent from the others, without taking into account kinematic constraints. Exploiting this kind of approach Zhou in [12] uses a KF to correct the gravity and Earth magnetic field estimation with IMUs measurements and then uses them to estimate human limb attitude. Considering only one Degree of Freedom (DoF) for the arm the position error obtained is less than 1 cm, although accuracy is sensitive to measurement accuracy and physical dimensions of all corresponding segments. Roetenberg in [7] uses a KF to estimate and correct the orientation

errors obtained integrating inertial measurements to track the human full body. No accuracy or performance assessments are provided by the authors. The second family of approaches comprises the nonlinear Bayesian filters, such as Extended Kalman Filter (EKF), Unscented Kalman Filter (UKF) and Particle Filters (PF). Despite being more computationally expensive, these algorithms give the possibility to deal with more complex models integrating also kinematic constraints among limbs. Using this kind of approach Yun and Bachmann in [10] estimate the quaternions representing limbs orientation combining a QUEST algorithm [2], exploiting acceleration and Earths magnetic field, with an EKF that fuses the QUEST estimation with an orientation update based on the limbs angular velocity. Their model has 3 DoFs, for its validation each DoF estimation was compared to a tilt table measurements. A model based on UKF is presented by Gohary and McNames in [3]. The authors propose a 5 DoFs model for the human upper limb, estimating joint angles, velocities and accelerations. A spherical joint is used to model the human shoulder and two rotational joints to model the elbow. The estimation is done through an UKF filter, fusing accelerometers and gyroscopes data. Results obtained show an average RMS error of less than 8° and a cross correlation coefficient  $r \geq 0.95$  with the optical system for the joint angles. A similar approach applied to a more complex kinematic model is presented by the authors in [6]. In this model the potentiality of the UKF are exploited to estimate 7 DoFs, comprising scapula motions, for the human upper limb. A different approach is presented by Zhang in [11] where the quaternions representing the upper limbs orientation are estimated through a PF, taking also into account the geometrical constraints of the elbow joint. Only one DoF between upper arm and forearm is considered, obtaining less than 15° of error in the angle estimation.

A drawback of Kalman Filters is that each of the variables involved in the models is potentially correlated to all the others. Since both the state and measurements matrices can be made of nonzero elements, it is possible for each variable to have some correlation with each of the others. The structure of the Kalman Filter indeed does not allow to directly represent variables independence. From this point of view, other probabilistic frameworks are more flexible for representing variables relations. Probabilistic Graphical Models (PGMs) provide such flexibility as they allow to define explicitly which variables are related and which are independent, thus making the estimation assumptions more realistic. Graphical models have been used in the field of motion tracking for both estimating human position and

<sup>1</sup>Emanuele Ruffaldi is with PERCRO, Tecip Institute, Scuola Superiore Sant'Anna, 56100 Pisa, Italy e.ruffaldi@sssup.it

motion analysis. In [4] the body was modeled as a kinematic chain and a 3D surface mesh and the system is represented with a dynamic Bayesian network. This framework is applied for reconstructing the body pose from a stream of monocular depth images. The body configuration is inferred through MAP inference. First the configuration at time  $t$  is generated from configuration at time  $t - 1$  through hill-climbing, then the evidence is applied detecting body parts from the optical stream, a set of correspondence between estimated and detected body parts is generated. At this point the evidence is iteratively propagated for every correspondence to find a new body configuration. Lastly hill-climbing is applied again to refine the estimation. It is to be noted that the inverse kinematic of the model, to estimate body part positions, is performed through MAP inference on a model linearized using Unscented Transformation (UT). In [1] a Bayesian Network was employed to fuse EMG biosignals with the dynamic model of an exoskeleton to estimate the applying torque of the human operator. Every variable is treated as a Gaussian process, and the posterior probability of the human applying torque is inferred from the network. As it can be seen PGM are particularly suitable for human motion analysis and for fusing information from a wide number of different sources. Due to the graphical structure the topology and the variable dependencies can be easily visualized and the Bayesian reasoning can be simplified with respect to the equivalent Kalman Filters.

In this work we propose a novel approach to motion reconstruction based on PGM. The structure of the human kinematics makes the PGM framework particularly suitable for exploiting IMUs sensors measurements and we show an example of how to apply PGM to human motion reconstruction. We indeed present two PGMs that aims at reconstructing body pose and motion based on IMUs signals and we choose two of them for the evaluation. We show that these models perform slightly better than state of the art Kalman Filters based models.

The paper is organized as follows. In section II is given a detailed description of how the problem is modeled from a kinematic and probabilistic view point. Section III describes the experimental setup carried on to test our approach, results are discussed in section V. Section VI concludes our contributions and explains future works.

## II. METHODS

### A. Arm kinematics

The human upper limbs are represented as a 5 DoFs kinematic chain rooted in the humerus head center with the shoulder providing 3 rotational DoFs (it is modeled as a spherical joint) and the elbow one flexion-extension DoF. The fifth DoF is the forearm pronation-supination. In the motion tracking field human motion has been often successfully addressed using techniques borrowed from robotic manipulator theories. The human upper limb can be represented as a chain of consecutive limbs parametrized using the DH convention. According to this convention a first frame  $i$  is attached to each limb, each frame  $z$  axis is coincident with the  $i+1$ -th

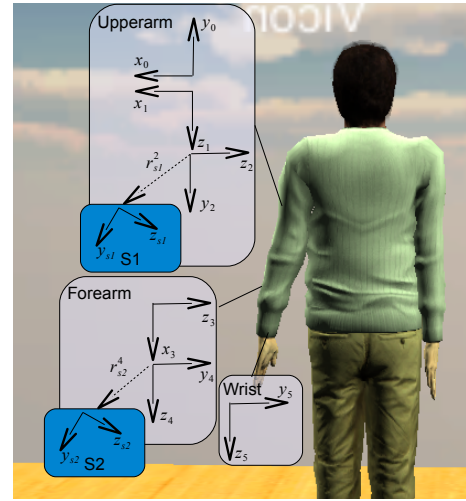


Fig. 1. Kinematic model for the human left arm using the DH convention. The shoulder is modeled with a spherical joint and the elbow with two rotational joints. Every joint frame is represented along with the sensors frames.

joint axis. A  $4 \times 4$  homogeneous matrix relates each frame to the following one. The  $i$ -th homogeneous matrix depends on four parameters, namely  $a_i$ ,  $\alpha_i$ ,  $d_i$ ,  $\vartheta_i$ . The parameter  $d_i$  represents translation between frames along  $z_{i-1}$  axis,  $\vartheta_i$  the rotation around  $z_{i-1}$  axis necessary to align  $x_{i-1}$  and  $x_i$ ,  $a_i$  is the translation along the  $x_i$  axis and,  $\alpha_i$  the rotation around  $x_i$  axis to align  $z_{i-1}$  with  $z_i$ . According to this the transformation matrix between link  $i - 1$  and link  $i$  is:

$$T_i^{i-1} = \begin{bmatrix} c_{\vartheta_i} & -s_{\vartheta_i}c_{\alpha_i} & s_{\vartheta_i}s_{\alpha_i} & a_i c_{\vartheta_i} \\ s_{\vartheta_i} & c_{\vartheta_i}c_{\alpha_i} & -c_{\vartheta_i}s_{\alpha_i} & a_i s_{\vartheta_i} \\ 0 & s_{\alpha_i} & c_{\alpha_i} & d_i \\ 0 & 0 & 0 & 1 \end{bmatrix} \quad (1)$$

where  $c_\psi$  and  $s_\psi$  are respectively  $\cos(\psi)$  and  $\sin(\psi)$ . According to this choice the kinematics can be represented by a list of joints and their parents, sensors are placed as ramifications. We follow the convention that a segment or sensor  $s$  is attached to a parent reference frame  $p$  and it is affected by the joint variables  $p + 1$ . Taking into account the use of inertial sensors, measuring angular velocity ( $\omega$ ), linear acceleration comprising the gravity vector ( $\ddot{x}$ ) and Earth magnetic field ( $m_i$ ), the previous convention leads to the following governing equations:

$$\begin{aligned} \omega_i &= R_p^i(\omega_p + \dot{q}_{p+1}z_0) \\ \dot{\omega}_i &= R_p^i(\dot{\omega}_p - \dot{q}_{p+1}S(z_0)\omega_p + \ddot{q}_{p+1}z_0) \\ \ddot{x}_i &= R_p^i\ddot{x}_p - S(r_{p,i}^i)\dot{\omega}_i + S(\omega_i)^2 r_{p,i}^i + g_i \\ g_i &= R_p^i g_p \\ m_i &= R_p^i m_p \end{aligned} \quad (2)$$

where we use the convention for vectors with pedex as the entity, and the apex as the reference system. When the apex is missing it is the same as the pedex: e.g.  $\omega_p^i$  is the angular velocity of joint  $p$  expressed in reference system  $i$ . For the transformations we use  $R_i^j$  to express the transformation from a vector in reference system  $i$  to reference system

$j$ . In the case of a sensors the  $\ddot{x}_s$  measure contains also a local gravity contribution  $g_i$ . We also remember the property  $S(\omega)^2 = -S(\omega)S(\omega)^T$ , where  $S(v)$  is the skew-matrix obtained from vector  $v$ . The  $i$ -th joint variables are expressed as  $q_i$ , corresponding with  $\vartheta_i$  in the DH convention,  $\dot{q}_i$  and  $\ddot{q}_i$ . The  $r_{p,i}^i$  is obtained from  $R_i^p t_i^p$ , where  $t_i$  is the translation component of the transformation from the  $i$ -th DH matrix.

$$t_i = \begin{bmatrix} a_i \\ d_i \sin(\alpha_i) \\ d_i \cos(\alpha_i) \end{bmatrix} \quad (3)$$

$$x_i = [q_i, \dot{q}_i, \ddot{q}_i]^T \quad i = 1, 2, \dots, n \quad (4)$$

Accordingly we define

$$x_{ab} = [x_a^T \dots x_b^T]^T \quad (5)$$

The equations 2 can be written by means of a general recursive formulation. A variable  $x_i$  is related to the parent as:

$$x_i = A_p^i x_p + b_i, \quad (6)$$

hence

$$x_i = \sum_{k=1}^p A_k^i b_k + b_i. \quad (7)$$

For example in the case of  $\omega$  we have  $A_i = R_p^i$  and  $b_i = \dot{q}_{p+1} z_0$ . Said

$$z_{S_i} = \begin{bmatrix} m_{S_i} \\ \omega_{S_i} \\ \ddot{x}_i \end{bmatrix} \quad (8)$$

the vector of sensor  $S_i$  measurements, equation 7 allows to write the measurements of the two sensors as functions of the joint variables:

$$z_{S1} = h_1(x_{13}) \quad (9)$$

$$z_{S2} = h_2(x_{15}) \quad (10)$$

that we will use for injecting the evidence provided by the sensors into the model.

### B. PGM Representation

Equations 2, 7, and 9 provide several ways to represent human arm kinematics. Equation 2 allows to represent the whole (serial) kinematic chain in a recursive way. The same chain can be represented as a directed acyclic graph (DAG). Fig. 2 shows the graph for 1 DoF.

When dealing with more complex models, it is convenient to use the compact representation shown in Figure 3, where all the variables related to the same joint are collapsed in one node as well as all the measures of the one sensor. Given the 1 DoF model, we developed the 5 DoFs model representing the human upper limb, shown in Figure 1. The 5 DoFs DAG is hence represented in Figure 4.

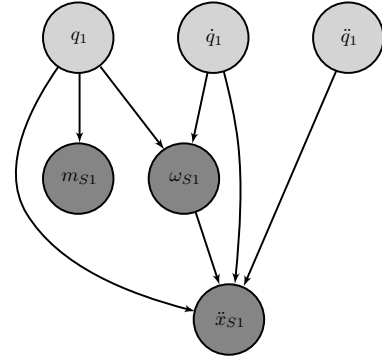


Fig. 2. Graphical Model for 1 dof model with 1 sensor attached. Light gray circles corresponds to variables, dark gray circles are observed variables.  $m_{S1}$  represents the Earth magnetic field sensed  $\omega_{S1}$  represents the angular velocity and  $\ddot{x}_{S1}$  the linear acceleration measured by the sensor.

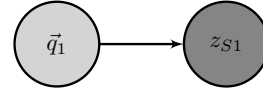


Fig. 3. DAG representation for 1 dof with 1 sensor in compact form, with all relative variables collapsed. The node with  $q_1$  comprehend  $q_1$ ,  $\dot{q}_1$  and  $\ddot{q}_1$ , while  $z_{S1}$  includes  $\omega_{s1}$ ,  $m_{s1}$  and  $\ddot{x}_{s1}$ . Light gray circles corresponds to variables, dark gray circles are observed variables.

### C. Message passing

This section shows the algorithms and the operations needed to obtain the marginal distributions of the variables of interests, i.e. joint variables  $q$ . We assume each variable of the graph to be drawn from a Gaussian distribution, thus having  $w \sim N(\mu_w, \Sigma_w)$  in normal, or, equivalently,  $w \sim N(y_w, Y_w)$  in canonical form. We will make use of both forms in the following, the transformation of one into the other is given by equation 11:

$$Y_w = \Sigma_w^{-1} \quad (11)$$

$$y_w = Y_w \mu_w \quad (12)$$

In the following we will use this notation: given a variable  $w$  and two time steps  $k-1$  and  $k$ , we indicate with  $w_k^-$  the value of  $w$  calculated from  $w_{k-1}$  before applying evidence from the sensors. We call  $\hat{z}_{S_i}$  the captured measurements of sensor  $S_i$  and we call  $Q_{S_i}$  the covariance matrix we associate to the measurements.

1) *Algorithms*: Once initialized (e.g. equal to zero) all the variables, we perform the *S2S1* algorithm here reported when acting between time steps  $k-1$  and  $k$ :

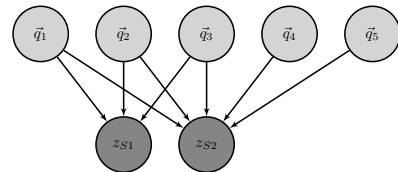


Fig. 4. DAG representation for 5 DoFs with 2 sensors in compact form, with all relative variables collapsed. Light gray circles corresponds to variables, dark gray circles are observed variables.

- 1) temporal update of root variables, i.e. joint variables and their derivatives:

$$[\mu_{x_{15_k}}^-, \Sigma_{x_{15_k}}^-] = \text{TempUpdate}(\mu_{x_{15_{k-1}}}, \Sigma_{x_{15_{k-1}}}) \quad (13)$$

- 2) Prediction of sensor  $S2$  measurements  $z_{S2}$  based on  $x$  temporal update:

$$[z_{S2_k}^-, Y_{x_{15_k} z_{S2_k}}^-] = \text{UT Transform}(x_{15_k}^-, h_2(x_{15_k}^-)) \quad (14)$$

In terms of message passing, referring to the figure 4 graph, this is the message that the  $x_1 x_2 x_3 x_4 x_5$  nodes send to  $z_{S2}$ .

- 3) Update of the  $x_{15}$  estimation based on sensor  $S2$  evidence  $\hat{z}_{S2}$  and measurements prediction by means of an unscented transformation:

$$[y_{x_{15_k}} Y_{x_{15_k}}] = \quad (15)$$

$$\text{UT Update}(y_{x_{15_k}}^-, Y_{x_{15_k}}^-, z_{S2_k}^-, Y_{x_{15_k} z_{S2_k}}^-, Q_{S2}, \hat{z}_{S2}) \quad (16)$$

This step comprises the message the  $z_{S2}$  node sends to itself as to inject evidence in the graph and the summation of the  $x_{15}^-$  and evidence messages.

- 4) Marginalization of  $x_{13}$  from  $x_{15}$  of step 3:

$$[y_{x_{13}}, Y_{x_{13}}] = \text{Marginalize}(y_{x_{15}}, Y_{x_{15}} \{1, 2, 3\}) \quad (17)$$

- 5) Prediction of sensor  $S1$  measurements based on updated  $x_{13}$  from step 3

$$[z_{S1_k}^-, Y_{x_{13_k} z_{S1_k}}^-] = \text{UT Transform}(x_{13_k}^-, h_1(x_{13_k}^-)) \quad (18)$$

- 6) Update of the  $x_{13}$  estimation based on sensor  $S1$  evidence  $\hat{z}_{S1}$  and measurements prediction:

$$[y_{x_{13_k}} Y_{x_{13_k}}] = \quad (19)$$

$$\text{UT Update}(y_{x_{13_k}}^-, Y_{x_{13_k}}^-, z_{S1_k}^-, Y_{x_{13_k} z_{S1_k}}^-, Q_{S1}, \hat{z}_{S1}) \quad (20)$$

By transforming  $y_{x_{13_k}}$  and  $y_{x_{15_k}}$  into normal form we obtain the desired marginals  $x_{15}$ . In order to refine their estimation, we may add another application of  $S2$  evidence based on the new estimation of  $x_{13}$  to obtain the  $S2S1S2$  algorithm, that is adding the following steps

- 7) Prediction of sensor  $S2$  measurements based on updated  $x_{15}$ :

$$[z_{S2_k}^-, Y_{x_{15_k} z_{S2_k}}^-] = \text{UT Transform}(x_{15_k}^-, h_2(x_{15_k}^-)) \quad (21)$$

- 8) Update of the  $q$  estimation based on sensor  $S2$  evidence  $\hat{z}_{S2}$  and measurements prediction by means of an unscented transformation:

$$[y_{x_{15_k}} Y_{x_{15_k}}] = \quad (22)$$

$$\text{UT Update}(y_{x_{15_k}}^-, Y_{x_{15_k}}^-, z_{S2_k}^-, Y_{x_{15_k} z_{S2_k}}^-, Q_{S2}, \hat{z}_{S2}) \quad (23)$$

The latter two steps can be repeated with sensors  $S1$  and  $S2$  to refine the estimation, however it is not guaranteed this iterative process to converge to a better estimation.

- 2) *operations*: Here we explain the operations underlying the steps of both algorithms.

**TempUpdate.** Given the model of  $x_i$  evolution in time (see equation 24) that we assume to be affected by white noise  $\nu$  whose covariance matrix is  $R$ , we first perform a *temporal update* on the root variables between time steps  $k-1$  and  $k$ , that is all the variables related to a joint are updated as

$$x_{i_k}^- = \begin{bmatrix} q_{i_k} \\ \dot{q}_{i_k} \\ \ddot{q}_{i_k} \end{bmatrix} = \begin{bmatrix} 1 & T_s & \frac{1}{2}T_s^2 \\ 0 & 1 & T_s \\ 0 & 0 & 1 \end{bmatrix} \begin{bmatrix} q_{i_{k-1}} \\ \dot{q}_{i_{k-1}} \\ \ddot{q}_{i_{k-1}} \end{bmatrix} + \nu = Ax_{i_{k-1}} + \nu \quad (24)$$

where  $T_s$  is the sample time (time interval between  $k-1$ -th and  $k$ -th samples). Accordingly, we update  $x_i$  covariance matrices as

$$\Sigma_{x_{i_k}}^- = A\Sigma_{x_{i_{k-1}}} A^T + R. \quad (25)$$

**UT Transform.** We exploit the unscented transformation [5], [9] to predict measurements based on the updated state. We select  $n$  sigma points  $X$  from  $x$  distributions and generate weights accordingly. The sigma points are transformed by means of equation 9 to have a sample  $Z$  of the target distribution, that, as assumed when applying UT, is still Gaussian. The UT transformation provides a prediction  $z^-$  of the measurements and the information matrix  $Y_{xz}^-$  of the state and the measurements, where all the variables are written in canonical form.

**UT Update.** Given  $z^-$ ,  $y_x^-$  and  $Y_{xz}^-$ ,  $y_x$  are linearly updated by exploiting evidence  $\hat{z}$ :

$$y_x = y_x^- + Y_x^- Y_{xz}^- Q^{-1} (\hat{z} - z^- + Y_{xz}^T y_x^-) \quad (26)$$

$$Y_x = Y_x^- Y_{xz}^- Q^{-1} Y_{xz}^T Y_x^- \quad (27)$$

thus allowing to push evidence towards  $x$ . It suffices to transform  $y$  canonical expressions into normal  $\mu$  to have the desired marginals of  $q_i$ ,  $\dot{q}_i$  and  $\ddot{q}_i$ .

**Marginalization**, that we report in canonical form. Given a variable  $y$  with information matrix  $Y$ , let  $s$  be the set of indices of  $y$  to keep in the marginalization and  $t$  the remaining ones to be marginalized out, we have

$$\tilde{Y} = Y(s, s) - Y(s, s)Y(t, t)^{-1}Y(s, t) \quad (28)$$

$$\tilde{y} = y(s) - Y(s, t)Y(t, t)^{-1}y(t) \quad (29)$$

where  $Y(s, s)$  is the submatrix of  $Y$  in which only the rows and columns in  $s$  are kept and  $\tilde{y}$  and  $\tilde{Y}$  are  $y$  and  $Y$  after marginalization.

### III. EXPERIMENT

We tested the proposed algorithms in two steps. Firstly, we tested the algorithms with simulated data. We generated joint trajectories reported in equations 30 to produce sensor measures.

$$\begin{aligned} q_1(t) &= \cos(\gamma t)^2 + \sin(2\gamma t)^2 \\ q_4(t) &= \cos(\gamma t)^2 + \cos(2\gamma t)^2 \\ q_2(t) &= \cos(\gamma t) \\ q_3(t) &= 0 \\ q_5(t) &= -\sin(\gamma t) \end{aligned} \quad (30)$$



Fig. 5. Experimental setup with the IMUs mounted on the participants limb as well as the Vicon system markers.

We calculated sensors  $S_1$  and  $S_2$  outputs according to equation 2. We considered  $S_1$  and  $S_2$  to be aligned to the limbs they are attached to, thus having  $R_{s1}^3 = R_{s2}^5 = I_3$ . Synthetic data sensors have been generated with random noise for 10 iterations and the algorithms have been tested iteratively. The results have been averaged among all the simulations.

The second validation step involved real measures that were obtained from a healthy male volunteer who wore two Bluetooth Invensense MPU9150 IMUs (Invensense, Borregas Ave Sunnyvale, CA, USA) on the upper arm and on the forearm respectively. He was asked to perform a sequence of movements that were captured by both the IMUs and the Vicon optical motion capture system (Vicon Oxford 14 Minns Business Park West Way Oxford, UK). Optical tracking provided ground truth data to compare UKF and PGM algorithms. Sensors data were collected at a rate of 100 Hz. The algorithms were implemented in Matlab<sup>®</sup> and run at 100 Hz frequency. Six reflective markers allowed to reconstruct upper limbs kinematics:  $M_1$  on the manubrium sternal,  $M_2$  on the left acromion,  $M_3$  and  $M_4$  were placed on the lateral and medial epicondyle to determine ulna trochlear notch and humerus throchlea axis,  $M_5$  and  $M_6$  were attached to the styloid process of the ulna and of the radius respectively to have the scaphoid-pisiform axis. Two further markers were used to capture IMUs positions. IMUs and Vicon data were synchronized after the capturing session. Figure 5 shows the capturing setup.

The participant was firstly asked to carry out three calibration steps consisting of movements aimed at calibrating the magnetometers followed by the N-pose and the T-pose to calibrate the sensors orientations. In the N-pose the subject stands with his arms along the gravity and palms facing the body. In the T-pose the subject stands with horizontal arms in the frontal plane. Then, he was asked to performed a sequence of functional movements involving elbow flexion/extension, elbow pronation/supination, shoulder abduction/adduction, shoulder rotation, and shoulder flex-

ion/extension. Markers data were analyzed (see [8]) to obtain joint variables according to the kinematic model explained in section II.

#### IV. ANALYSIS AND RESULTS

In order to compare algorithm performance against optical data, for each joint variable  $q$  we define  $\check{q}$  the algorithm estimation and  $\bar{q}$  the variable reconstruction from optical data. For each variable we define the root mean square error as:

$$E_q = \frac{1}{N} \sqrt{\sum_{k=1}^N (\check{q}(k) - \bar{q}(k))^2} \quad (31)$$

where  $N$  is the number of samples that were captured.  $E_q$  allows to evaluate the overall error in the joint variable estimation given that the optical data are the ground truth. Another measurement of estimation goodness is the correlation of algorithm estimation with optical data reconstruction. We hence define the correlation coefficient

$$C_q = \frac{\sum_{k=1}^N (\check{q}(k) - \bar{q}) (\bar{q}(k) - \bar{q})}{\sqrt{\sum_{k=1}^N (\check{q}(k) - \bar{q})^2 \sum_{k=1}^N (\bar{q}(k) - \bar{q})^2}} \quad (32)$$

We first report in Table I results obtained in the first test synthetic data. As there was no risk of data misalignment, only the RMSE was calculated. The results for the test with

|                                    | S2S1   | S2S1S2 | UKF    |
|------------------------------------|--------|--------|--------|
| $q$ [rad]                          | 0.034  | 0.029  | 0.029  |
| $\dot{q}$ [rad/sec]                | 0.084  | 0.077  | 0.078  |
| $\ddot{q}$ [rad/sec <sup>2</sup> ] | 1.0782 | 0.9832 | 1.0243 |

TABLE I

AVERAGE OF THE  $E_q$ ,  $E_{\dot{q}}$  AND  $E_{\ddot{q}}$  FOR ALL THE JOINTS IN THE 5 DOFS KINEMATIC CHAIN WITH SYNTHETIC SENSORS MEASUREMENTS.

real measurements are reported in Table II and Table III. In Table II the comparisons among the RMSEs for every joint for the three algorithms are shown, whereas in the Table III the correlations between the estimation with our approach and the UKF with the optical estimation are reported. We

|             | S2S1  | S2S1S2 | UKF   |
|-------------|-------|--------|-------|
| $q_1$ [deg] | 6.68  | 6.78   | 6.84  |
| $q_2$ [deg] | 7.67  | 6.64   | 7.58  |
| $q_3$ [deg] | 3.81  | 3.77   | 3.80  |
| $q_4$ [deg] | 7.25  | 7.24   | 7.29  |
| $q_5$ [deg] | 15.47 | 15.49  | 15.50 |

TABLE II

$E_q$ ,  $E_{\dot{q}}$  AND  $E_{\ddot{q}}$  FOR ALL THE JOINTS IN THE 5 DOFS KINEMATIC CHAIN WITH REAL SENSORS MEASUREMENTS.

finally report the estimation of the  $S2S1S2$  algorithm in figure 6 as an example of how these algorithms perform.

|       | S2S1 | S2S1S2 | UKF  |
|-------|------|--------|------|
| $q_1$ | 0.94 | 0.94   | 0.93 |
| $q_2$ | 0.81 | 0.81   | 0.80 |
| $q_3$ | 0.98 | 0.98   | 0.98 |
| $q_4$ | 0.98 | 0.98   | 0.98 |
| $q_5$ | 0.75 | 0.74   | 0.74 |

TABLE III

$C_q$ ,  $C_{\dot{q}}$  AND  $C_{\ddot{q}}$  FOR ALL THE JOINTS IN THE 5 DOFS KINEMATIC CHAIN WITH REAL SENSORS MEASUREMENTS.

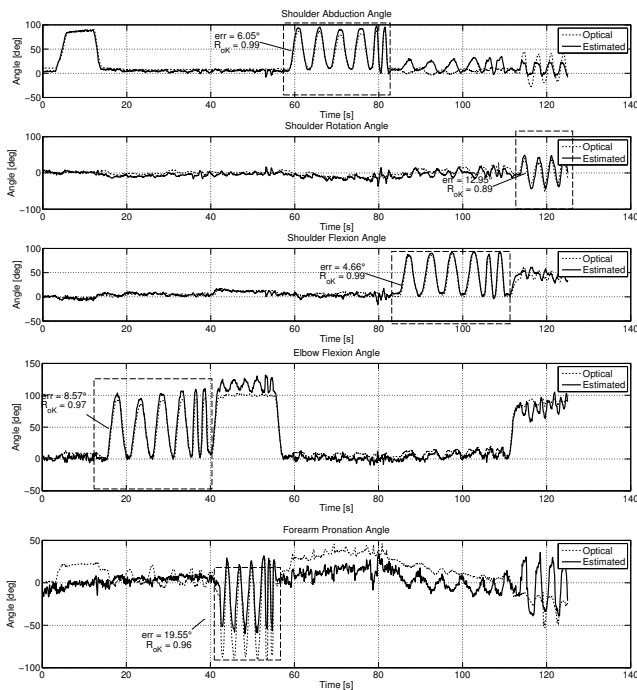


Fig. 6. Motion tracking results obtained with the S2S1S2 algorithm. The DoF-related functional movements are highlighted by the boxes.

## V. DISCUSSION

From the experimental setup it can be seen that as far as synthetic measures are concerned the iterated message passing algorithm shows the same results of the UKF for  $q$  and  $\dot{q}$ , while there is a slight improvement in the  $\ddot{q}$  estimation. The basic message passing algorithm performs instead slightly worse than the UKF. Results from real data show that while the message passing algorithm has an overall performance equal to the UKF, the iterated message passing algorithm performs slightly better with an increment of accuracy of  $1^\circ$  on the shoulder rotation estimate. Although errors in optical estimation of joint angles may have arisen questions about the validation, the high values of correlation between the different algorithms and the optical estimation allow to conclude for the validity of the experiment. It is to be noted that although the current implementation of the algorithm preserves the sensors independence, joints variables can be correlated each other. This happens because the sensor S2 output is determined by all the 5 DoFs of the kinematic chain. During the collection of the evidence from the leaf to the root

we obtain a full covariance matrix, leading to dependencies among state variables belonging to different joints.

## VI. CONCLUSIONS

In this work we presented a novel approach to human motion reconstruction with IMUs that exploits PGMs. The model represents better the actual dependencies of the variables compared to Kalman Filters. We proposed a message passing algorithm and an iterated message passing algorithm to infer joints variable from sensor measurements. The results of the two algorithms have been compared to the ones of a UKF, widely used in the state of the art, both with synthetic and real measurements data. The results showed that there is a slight improvement in the estimation using the iterated message passing algorithm. As far as future developments are concerned, we are actually working at refining the message passing algorithm to maintain also the independence among different joints variables and increase the estimates accuracy. An additional aspect that will be considered is the computational cost, to make the algorithm suitable for real-time embedded motion tracking.

## REFERENCES

- [1] C.-A. Cheng, T.-H. Huang, and H.-P. Huang. Bayesian human intention estimator for exoskeleton system. In *Advanced Intelligent Mechatronics (AIM), 2013 IEEE/ASME International Conference on*, pages 465–470. IEEE, 2013.
- [2] Y. Cheng and M. D. Shuster. Robustness and accuracy of the quest algorithm. *Advances in the Astronautical Sciences*, 127:41–61, 2007.
- [3] M. El-Gohary and J. McNamara. Shoulder and elbow joint angle tracking with inertial sensors. *Biomedical Engineering, IEEE Transactions on*, 59(9):2635–2641, 2012.
- [4] V. Ganapathi, C. Plagemann, D. Koller, and S. Thrun. Real time motion capture using a single time-of-flight camera. In *Computer Vision and Pattern Recognition (CVPR), 2010 IEEE Conference on*, pages 755–762. IEEE, 2010.
- [5] D.-J. Lee. Unscented information filtering for distributed estimation and multiple sensor fusion. In *AIAA Guidance, Navigation and Control Conference and Exhibit*, 2008.
- [6] L. Peppoloni, A. Filippeschi, E. Ruffaldi, and C. A. Avizzano. A novel 7 degrees of freedom model for upper limb kinematic reconstruction based on wearable sensors. In *Intelligent Systems and Informatics, SISY. The 11th IEEE International Symposium on*, pages 105–110. IEEE, 2013.
- [7] D. Roetenberg, H. Luinge, and P. Slycke. Xsens mvn: full 6dof human motion tracking using miniature inertial sensors. Technical report, 2009.
- [8] D. Tolani, A. Goswami, and N. I. Badler. Real-time inverse kinematics techniques for anthropomorphic limbs. *Graphical models*, 62(5):353–388, 2000.
- [9] E. A. Wan and R. Van Der Merwe. The unscented kalman filter for nonlinear estimation. In *Adaptive Systems for Signal Processing, Communications, and Control Symposium 2000. AS-SPCC. The IEEE 2000*, pages 153–158. IEEE, 2000.
- [10] X. Yun and E. R. Bachmann. Design, implementation, and experimental results of a quaternion-based kalman filter for human body motion tracking. *Robotics, IEEE Transactions on*, 22(6):1216–1227, 2006.
- [11] Z.-Q. Zhang and J.-K. Wu. A novel hierarchical information fusion method for three-dimensional upper limb motion estimation. *Instrumentation and Measurement, IEEE Transactions on*, 60(11):3709–3719, 2011.
- [12] R. Zhu and Z. Zhou. A real-time articulated human motion tracking using tri-axis inertial/magnetic sensors package. *Neural Systems and Rehabilitation Engineering, IEEE Transactions on*, 12(2):295–302, 2004.